ACS Catalysis

Research Article

pubs.acs.org/acscatalysis

Interplay between Reaction Mechanism and Hydroxyl Species for Water Formation on Pt(111)

Rodrigo Ferreira de Morais,[†,‡] Alejandro A. Franco,[¶,§,□] Philippe Sautet,[†] and David Loffreda*[,†]

[†]Université de Lyon, CNRS, Ecole Normale Supérieure de Lyon, Institut de Chimie de Lyon, Laboratoire de Chimie, 46 Allée d'Italie, F-69364 Lyon Cedex 07, France

[‡]CEA, DRT/LITEN/DEHT/LCPEM, 17 Rue des Martyrs, F-38054 Grenoble Cedex 9, France

[¶]Laboratoire de Réactivité et Chimie des Solides (LRCS), Université de Picardie Jules Verne and CNRS, UMR 7314 - 33 Rue Saint Leu, F-80039 Amiens Cedex 1, France

[§]RS2E, Réseau sur le Stockage Electrochimique de l'Energie FR CNRS 3459, F-80039 Amiens Cedex 1, France

[□]ALISTORE-ERI, European Research Institute, FR CNRS 3104, F-80039 Amiens Cedex 1, France

Supporting Information

ABSTRACT: Predicting the reaction mechanism of water and hydrogen peroxide formation on a platinum catalyst is a crucial step toward the understanding of the corresponding selectivity in polymer electrolyte membrane fuel cells. In this perspective, the environment of the catalytic active site should play an important role; however, its explicit description at the atomic scale is an ongoing challenge for theoretical approaches. In this study, we propose to model three effects of the environment: surface hydroxyl coverage, temperature, and reactant pressure. A detailed investigation of the reaction mechanism of water and hydrogen peroxide formation on a platinum surface is reported on the basis of density functional theory (DFT) calculations and Gibbs free energy diagrams. In standard conditions of reaction (1 atm and 353 K), the selectivity toward water and hydrogen peroxide depends on the competition between two reaction paths (molecular oxygen direct dissociation and hydrogenation), which can be tuned by the partial coverage of OH intermediate. At a low coverage of 1/12 ML, the catalyst activity is expected to be low due to a preferential but activated direct oxygen dissociation. When the OH partial coverage increases, the hydroperoxyl route becomes favorable, hence leading to hydroxyl and water by the nonactivated OOH dismutation. The direct oxygen dissociation and the whole reaction mechanism are sensitive to the hydroxyl partial coverage. Our gas/metal model opens the way to new elementary mechanisms in the presence of aqueous electrolyte and electric field that would explain how water can be produced at the beginning of the reaction (at low coverage).

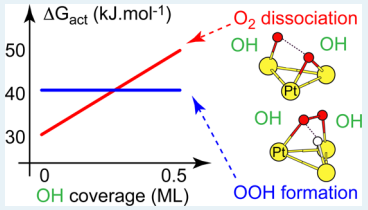

KEYWORDS: *catalytic water formation, density functional theory, free energy, activation energy, platinum, coverage effect, hydroxyl, hydrogen peroxide*

1. INTRODUCTION

Among the possible environmental solutions for future automotive applications is the development and the use of polymer electrolyte membrane fuel cells (PEMFCs). Unfortunately, the wide commercialization of such devices has been held back by various issues such as the cost of the platinum catalyst and the low durability caused by the degradation of materials.[1] To overcome the question of the catalyst loading, platinum-based alloys have been proposed in the literature as an alternative for keeping a reasonable catalytic activity toward oxygen reduction reaction (ORR).[2−6] Additionally, those difficulties have opened the way for various theoretical studies at the atomic scale, which are often limited with respect to the modeling of the complex environment of fuel cells (electrolyte, electric field, etc.).[7−23] For instance, a detailed analysis of the effect of surface coverage of hydroxyl (OH) species on thermodynamics and kinetics of ORR has not been reported so far on the basis of density functional theory (DFT).

In ORR, two different products, water (H_2O) and hydrogen peroxide (H_2O_2), are in competition. The second one may be responsible for the electromechanical degradation of the membrane, through a mechanism still without consensus in the community.[24−27] In idealistic conditions where the solvent and the electric field are neglected, the reaction mechanism is already complex. In most of the theoretical studies, two competitive elementary steps are often mentioned: water formation either through direct molecular oxygen dissociation or hydroperoxyl (OOH) formation.[15,28−37] According to Ford et al., at a coverage of 0.25 ML, the direct route is less favorable due to a succession of high activation barriers for the molecular dissociation (0.71 eV) and for OH formation via O + H (0.72 eV).[36] In contrast, the OOH-mediated route offers a sequence of low activation energies for O_2 + H association (0.29 eV) and O + OH dissociation (0.16 eV). Finally, for this coverage, the formation of hydrogen peroxide from OOH species is predicted to be disfavored due to a slightly larger barrier (0.21 eV) than

Received: August 22, 2014
Revised: December 10, 2014
Published: December 11, 2014

DOI: 10.1021/cs5012525
ACS Catal. 2015, 5, 1068−1077

OOH quasi-spontaneous dissociation into O + OH (0.16 eV). As soon as atomic oxygen is formed and the water is present on the catalyst surface (either produced by the reaction or coming from the solution), the disproportionation reactions between two H_2O molecules and one O may occur at an even higher coverage (3/4 ML) and may open an even less activated alternative mechanism for yielding OH surface intermediates (0.12 eV).[30] The effect of the increasing potential at room temperature is expected to change this picture significantly by generally increasing the activation barriers (loss of catalytic activity) and by poisoning the catalyst due to a stronger stability of adsorbed O and OH species.[36,38] These conclusions provided by Ford et al. are not entirely supported by other authors.[11] At low coverage, only a few DFT studies have oriented the discussion in this direction so far.[14,34,39−41] Qi et al. have questioned the relative order between the key activation barriers by demonstrating that oxygen dissociation is much easier at a low coverage of 1/16 ML (0.27 eV against 0.42 eV for OOH formation).[34] This trend is thus opposite to the picture proposed by Ford et al.[36] These studies demonstrate that adsorbate species surrounding the active site have a major influence on the barriers of the elementary steps. In many cases, the surface coverage is just modeled by changing the surface unit cell in a periodic calculation. This has strong limitations on the nature of the coadsorbate species, which has to be the periodic image of the reactant, and this is here evolving along the pathway. Thus, it is crucial to model the environment of the reactant species in a realistic way. In summary, in the theoretical context, most of the previously published works deal only with a restricted set of elementary steps related to ORR, at a model coverage of 1/4 ML. Three DFT studies of ORR on Pt(111) have been reported with a more complete description of the reaction mechanism but without varying the coverage of coadsorbed hydroxyl species. Hence a systematic theoretical investigation of a complete set of elementary acts as a function of reactant surface coverage is still missing so far.

In this work, we explore the reaction mechanism of water and hydrogen peroxide formation on a platinum surface on the basis of density functional theory calculations. A low coverage is first considered to investigate the elementary steps of the mechanism. The search of the transitions rates and corresponding activation energy barriers is reported at this coverage systematically. Second the reactivity study is extended to the situations where the reacting species are surrounded by hydroxyl groups on the surface. Several coverage of hydroxyl groups has been defined, and their influence on thermodynamics of intermediates and kinetics of the elementary steps is discussed. Then Gibbs free energy diagrams have been constructed to explore the competition between direct oxygen dissociation and hydroperoxyl formation in standard conditions of temperature and pressure of reactants, and as a function of the surface coverage of hydroxyl species.

2. METHODOLOGY

2.1. Computational Details. Throughout this study, the DFT calculations have been performed with VASP[42−44] in periodic boundary conditions. The generalized gradient approximation (GGA) has been used with the Perdew−Burke−Ernzerhof (PBE) exchange−correlation functional[45] and the projector augmented-wave method (PAW).[46] An energy cutoff of 400 eV has been considered for the expansion of the plane-wave basis set. Spin-polarized calculations have been performed mainly for the adsorption structures of molecular oxygen on platinum. The criterion for the convergence of total electronic energy has been set to 10^{-6} eV. Accurate geometry optimizations have been ensured by a tight threshold of 10^{-2} eV Å^{-1} for the residual forces acting on the nuclei. In this work, the low coverage has been modeled by a $(2\sqrt{3} \times 2\sqrt{3})$-R30° supercell corresponding to a formal coverage of θ_{tot} = 1/12 ML (ML = monolayer), as depicted in Figure 1. This coverage has been increased by considering

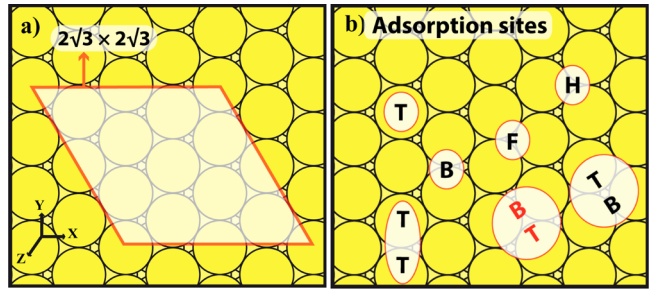

Figure 1. (a) Top view of the Pt(111) surface model, showing the $(2\sqrt{3} \times 2\sqrt{3})$-R30° supercell. (b) Definitions of key adsorption sites: T (Top), B (Bridge), F (hollow Fcc), H (hollow Hcp), TT (Top-Top), TB (Top-Bridge) above a fcc hollow position, BT (Bridge-Top) above a hcp hollow site.

coadsorption with hydroxyl species in the surrounding of the active site, in the same supercell. Therefore, three additional formal total coverage of θ_{tot} = 1/4 ML (2 OH, θ_{OH} = 1/6 ML), θ_{tot} = 5/12 ML (4 OH, θ_{OH} = 1/3 ML), θ_{tot} = 7/12 ML (6 OH, θ_{OH} = 1/2 ML) have been defined to explore their influence on the reactivity. The numerical integration in the Brillouin zone has been performed on a (3 × 3 × 1) Monkhorst−Pack k-point mesh.[47] The numerical error due to the k-point sampling has been evaluated by increasing the k-point density from (3 × 3 × 1) to (7 × 7 × 1) and is below 1 meV/atom. The numerical error due to the basis set has also been checked by increasing the energy cutoff (4 meV/atom). The Pt(111) surface has been modeled by a periodic slab composed of five metallic layers and a vacuum space of 14 Å in the z direction, normal to the surface. The systematic error of the model related to the thickness of the slab has been estimated by increasing the number of metallic layers up to 21 atomic planes in order to evaluate the convergence of the surface energy. Starting from nine-layer symmetric slabs (or five nonsymmetric models), the change of surface energy becomes negligible (below 1 meV Å^{-2}). Adsorption has been modeled on one side of five-layer nonsymmetric slabs. During the geometry optimizations, the degrees of freedom of the adsorbate and those of the three uppermost metallic layers have been relaxed, whereas the positions of two lowest platinum planes have been kept frozen in a bulk-like optimal geometry (Pt−Pt distance of 2.81 Å). The search of the transition states (TS) connecting the phase spaces of reactants and products and the generation of reaction pathways have been performed by a linear interpolation of the Cartesian coordinates. TS approximate structures have been determined with a set of eight intermediate geometries. For several delicate cases, 16 intermediate geometries have been necessary to approximate correctly the saddle-point (SP) region. The minimization of the reaction pathways has been performed by using the climbing-image Nudged Elastic Band (CI-NEB) method implemented in VASP.[48,49] For difficult cases for which the linear interpolation of Cartesian coordinates

DOI: 10.1021/cs5012525
ACS Catal. 2015, 5, 1068−1077

was not effectively working, the pathways have been generated by Opt'n Path with Baker coordinates.[50] The refinement of approximate TS geometry resulting from the CI-NEB method has been achieved by minimizing all the residual forces with a DIIS algorithm (quasi-Newton). Finally, the SP have been identified as transition states (first-order SP) with a vibrational analysis showing the existence of one normal mode associated with a pure imaginary frequency (as described later).

The technique for the vibrational analysis is based on the numerical calculation of the second derivatives of the potential energy surface within the harmonic approach (see[51] for details). In the vibrational treatment, only the degrees of freedom of the adsorbates have been included systematically (vibrational Γ point). Two points per degree of freedom (±0.02 Å) have been considered to evaluate each element of the Hessian matrix. The diagonalization of the force constant matrix provides the harmonic frequencies and the associated normal modes.

2.2. Reaction Mechanism. The reaction mechanism modeled in our study is composed of 14 elementary steps, detailed in the following:

$$H_{2(gas)} + 2(*) \rightarrow 2H_{(ads)} \quad \text{(A1)}$$

$$O_{2(gas)} + 2(*) \rightarrow 2O_{(ads)} \quad \text{(A2d)}$$

$$O_{2(gas)} + (*) \rightarrow O_{2(ads)} \quad \text{(A2m)}$$

$$O_{2(ads)} + (*) \rightarrow 2O_{(ads)} \quad \text{(S1)}$$

$$O_{(ads)} + H_{(ads)} \rightarrow OH_{(ads)} + (*) \quad \text{(S2)}$$

$$OH_{(ads)} + H_{(ads)} \rightarrow H_2O_{(ads)} + (*) \quad \text{(S3)}$$

$$2OH_{(ads)} \rightarrow H_2O_{(ads)} + O_{(ads)} \quad \text{(S4)}$$

$$2OH_{(ads)} \rightarrow H_2O_{2(ads)} + (*) \quad \text{(S5)}$$

$$O_{2(ads)} + H_{(ads)} \rightarrow OOH_{(ads)} + (*) \quad \text{(S6)}$$

$$OOH_{(ads)} + (*) \rightarrow OH_{(ads)} + O_{(ads)} \quad \text{(S7)}$$

$$OOH_{(ads)} + H_{(ads)} \rightarrow 2OH_{(ads)} \quad \text{(S8)}$$

$$OOH_{(ads)} + H_{(ads)} \rightarrow H_2O_{2(ads)} + (*) \quad \text{(S9)}$$

$$H_2O_{(ads)} \rightarrow H_2O_{(gas)} + (*) \quad \text{(D1)}$$

$$H_2O_{2(ads)} \rightarrow H_2O_{2(gas)} + (*) \quad \text{(D2)}$$

2.3. Gibbs Free Energy Calculations. In order to compare the adsorption properties of ORR intermediates, they have to be evaluated with a common reference. Because those intermediates have a different total number of oxygen and hydrogen atoms, we have chosen to define the global reference as follows:

$$O_{2,gas} + H_{2,gas} + (*) \rightarrow (O_aH_b)_{ads} + yO^{\infty}_{ads} + zH^{\infty}_{ads} \quad (1)$$

where $(O_aH_b)_{ads}$ corresponds to the various ORR adsorbed species, O^{∞}_{ads} and H^{∞}_{ads} to the required number of adsorbed atomic oxygen and hydrogen at an infinite position:

$$a + y = 2 \quad (2)$$

$$b + z = 2 \quad (3)$$

The common reference being defined, the effect of OH surface coverage is introduced in our model as follows:

$$\mathcal{N}_1O_{2,gas} + \mathcal{N}_2H_{2,gas} + (*) \rightarrow (O_{n_1}H_{n_2} + xOH)_{coads} \quad (4)$$

where $(O_{n_1}H_{n_2} + xOH)_{coads}$ defines the coadsorption states between ORR intermediates and additional OH surface species, by varying the number x of OH from 0 to 6 in the supercell:

$$2\mathcal{N}_1 = n_1 + x = (a + y) + x = 2 + x \quad (5)$$

$$2\mathcal{N}_2 = n_2 + x = (b + z) + x = 2 + x \quad (6)$$

The Gibbs free energy of reactive coadsorption ΔG_{rcoads} per unit cell area $\mathcal{A}$ is defined from the following equation for initial (IS), transition state (TS) and final state (FS) of each elementary step. In this thermodynamic model, the gas phase plays the role of a reservoir in equilibrium with the adsorbed layer on the platinum surface, hence imposing its pressure and temperature. Within those assumptions, ΔG_{rcoads} reads:

$$\Delta G_{rcoads} = (G_{coads} - G_{(*)} - \mathcal{N}_1\mu_{O_{2,gas}} - \mathcal{N}_2\mu_{H_{2,gas}})/\mathcal{A} \quad (7)$$

$$= (F_{conf,coads} + \Delta E_{rcoads} - k_BT\ln[(Z^0_{coads})\left(\frac{P_{tot}R/(R+1)}{k_BTZ^0_{trs,O_{2,gas}}Z_{rot,O_{2,gas}}}\right)^{\mathcal{N}_1}\left(\frac{P_{tot}/(R+1)}{k_BTZ^0_{trs,H_{2,gas}}Z_{rot,H_{2,gas}}}\right)^{\mathcal{N}_2}])/\mathcal{A} \quad (8)$$

where the exponents $\mathcal{N}_1$ and $\mathcal{N}_2$ are affine functions of x, as demonstrated in eq 5 and 6. Thus, they contain in part the dependence of ΔG_{rcoads} on x. G_{coads} and $G_{(*)}$ are the Gibbs free energies of the coadsorbed system and the clean metallic surface. $\mu_{O_{2,gas}}$ and $\mu_{H_{2,gas}}$ are the chemical potentials of the gas phase reference molecules. $F_{conf,coads}$ is the configurational Helmoltz energy of the coadsorbed phase, calculated as follows:

$$F_{conf,coads} = -k_BT\ln\left(\frac{N_{site}!}{(N_{site} - N_{coads})!N_{coads}!}\right) \quad (9)$$

in which N_{site} and N_{coads} are the number of free surface sites and the number of coadsorbed species, respectively. N_{coads} is also an affine function of x.

In eq 8, ΔE_{rcoads} is the reactive coadsorption energy obtained by the difference between the total electronic energy of the coadsorbed system and those of the clean platinum surface and gas phase references. Z^0_{coads} is the total partition function of the coadsorbed system (essentially the vibrational partition function). $Z^0_{trs,O_{2,gas}}$ and $Z^0_{trs,H_{2,gas}}$ are the 3D translational partition functions for the gas phase references. In this formulation, Z^0 means that they depend only on temperature. $Z_{rot,O_{2,gas}}$ and $Z_{rot,H_{2,gas}}$ are the rotational partition functions of the gas phase molecules (see, for instance, ref 52 for more details). The vibrational entropy variation is neglected here in a first approximation. P_{tot} and R are the total pressure $(P_{O_2} + P_{H_2})$ and the ratio between oxygen and hydrogen partial pressure (P_{O_2}/P_{H_2}), respectively.

3. DENSITY-FUNCTIONAL THEORY CALCULATIONS

3.1. Low Coverage Analysis. In this section, we present the DFT results related to the elementary steps composing the

DOI: 10.1021/cs5012525
ACS Catal. 2015, 5, 1068−1077

Table 1. Forward (fwd) and Backward (bwd) Activation Energies E_{act} and Reaction Energies ΔE_{reac} (Total Electronic Energies in kJ mol^{-1}) of the Elementary Steps of Water and Hydrogen Peroxide Formations on Pt(111), against Hydroxyl Coverage (θ_{OH}, ML)

elementary act	E_{act}^{fwd} (kJ mol^{-1})				E_{act}^{bwd} (kJ mol^{-1})				ΔE_{reac} (kJ mol^{-1})			
θ_{OH} (ML)	0	1/6	1/3	1/2	0	1/6	1/3	1/2	0	1/6	1/3	1/2
(S1) $O_{2(ads)} \rightarrow 2O_{(ads)}$	30	31	44	51	149	137	150	150	−119	−106	−106	−99
(S6) $O_{2(ads)} + H_{(ads)} \rightarrow OOH_{(ads)}$	38	35	40	35	42	56	53	56	−3	−21	−13	−21
(S2) $O_{(ads)} + H_{(ads)} \rightarrow OH_{(ads)}$	88	90	84	80	94	100	108	115	−6	−10	−24	−34
(S3) $OH_{(ads)} + H_{(ads)} \rightarrow H_2O_{(ads)}$	19	16	15	23	80	85	94	157	−61	−69	−78	−133
(S9) $OOH_{(ads)} + H_{(ads)} \rightarrow H_2O_{2(ads)}$	24	33	23	–	46	52	57	–	−23	−18	−34	–
(S7) $OOH_{(ads)} \rightarrow OH_{(ads)} + O_{(ads)}$	0	5	4	–	158	156	199	–	−159	−152	−195	–
(S4) $2OH_{(ads)} \rightarrow H_2O_{(ads)} + O_{(ads)}$	1	5	5	–	24	25	26	–	−24	−20	−21	–

reaction mechanism of water and hydrogen peroxide formations on Pt(111), at a low coverage (1/12 ML). In Table 1, the calculated forward and backward activation barriers and corresponding reaction energy have been exposed for each elementary act. The top and lateral views of initial, transition, and final optimized states have been reported in Figure 2 and 3 for each elementary act (the definition of the adsorption sites being presented in Figure 1). A first general remark concerns the elementary steps of the reaction mechanism. Among the list of the nine surface transformations (S_i), two of them are not elementary acts: S5 hydrogen peroxide dismutation and S8 hydroperoxyl comproportionation. In the case of S5, several configurations of the initial state have been optimized. However, none of them could have been considered to build an effective reaction pathway. The simple reason is the stabilizing hydrogen bond that can be formed between two neighboring coadsorbed hydroxyl species, hence giving a chemical sequence (H−O−H-O) opposite to the one expected to form hydrogen peroxide (H−O−O-H). In the case of S8, the simultaneous association of atomic hydrogen and hydroperoxyl (S2-type) with hydroperoxyl dismutation (S7-type) implies that both events are sufficiently activated and their thermicities have to be moderate (close to athermicity). However, we will see later in the analysis that S7 is not activated and largely exothermic, hence S8 could not be an elementary step, in disagreement with Qi et al.,[34] who evaluated an activation barrier for S8 of 30 kJ mol^{-1} from a coadsorption state between two neighboring OH species (not a transition state). The second remark is related to the large change of thermicity of the remaining seven possible elementary acts. As shown in Table 1, the reaction energies of those steps are all exothermic. Nonetheless, two of them (oxygen dissociation S1 and hydroperoxyl dismutation S7) are strongly exothermic. This difference is essentially due to the balance of the number of formed platinum-atomic oxygen bonds which are intrinsically strong (+3 bonds for S1 and +2 bonds for S7). Another general remark concerns the order of magnitude of the forward and backward activation barriers of all the elementary steps. According to our low coverage model, most of the forward activation energies are weak or moderate (in the range 0−38 kJ mol^{-1}). There is one exception (S2 OH formation) for which the forward barrier is twice larger (88 kJ mol^{-1}). In contrast, for backward barriers, half of them are large (80−158 kJ mol^{-1}), the rest of the list being moderate (24−46 kJ mol^{-1}). Regarding the optimal geometries of the transition states, most of the low coverage structures proposed in Figure 2 and 3 are consistent with previous DFT studies at medium or high coverage.[28,29,33,34,36,53] There is again one exception related to hydrogen peroxide formation that will be discussed here below.

According to the reaction profile exposed in Figure 4, the dissociative adsorption of hydrogen (2) and the molecular adsorption of oxygen (3) are both exothermic on Pt(111) with respective DFT values of −98 and −73 kJ mol^{-1} at a low coverage of 1/12 ML. Starting from adsorbed oxygen, two elementary steps can occur simultaneously: direct oxygen dissociation S1 and hydroperoxyl formation S6. In fact, they exhibit similar activation barriers (30 and 38 kJ mol^{-1}, respectively), although the imaginary frequencies are different (66 and 779 cm^{-1}, respectively). This contrasts with previous works at medium and high coverage where the barrier for oxygen dissociation (60−74 kJ mol^{-1})[13,33,36,53] is larger than that of hydroperoxyl formation (28−41 kJ mol^{-1}).[34,36] However, our finding is in good agreement with Qi et al.'s previous work at low coverage for oxygen dissociation[34] (26−36 kJ mol^{-1}) and agrees with Hyman et al.[54] (19 kJ mol^{-1}). Another interesting difference with Qi et al.'s calculations is the intrinsic nature of the reaction pathway and transition states. According to their model in a ($2\sqrt{3} \times 4$) supercell (1/16 ML), molecular oxygen dissociates either over a TT position or over a TB site, as far as one can see from their reported results. In our study, we could not find a pathway allowing the dissociation over a TT form, after several attempts. In fact, we have registered along the NEBs a systematic prior diffusion from TT to TB structures before dissociation. Regarding oxygen dissociation, a final remark concerns the comparison with the experimental literature. Our barrier nicely agrees with STM measurements of single molecular oxygen at low coverage showing a dissociation barrier of 34−37 kJ mol^{-1}[55] and also with molecular beam and electron energy loss spectroscopy techniques (28 kJ mol^{-1}).[56] Regarding hydroperoxyl formation (5′), only comparison with previous theoretical results can be done. Our activation barrier of 38 kJ mol^{-1} and transition state structure (cf. Figure 3) at a low coverage of 1/12 ML are consistent with other DFT studies at a larger coverage of 1/4 ML (28−41 kJ mol^{-1}).[34,36] Hence, the change of the reactant coverage has a different effect on the activation energies. The barrier of the direct oxygen dissociation is sensitive to the surface coverage of adsorbed molecular oxygen, whereas that of hydroperoxyl formation is not depending on OOH coverage.

The next step in the reaction profile is the formation of the hydroxyl intermediate (7). The first two possible routes are either from O + H association (S2, with a barrier of 88 kJ mol^{-1} and an imaginary frequency of 819 cm^{-1}), or OOH dismutation (S7, with no activation barrier and an imaginary frequency of 286 cm^{-1}). S2 exhibits the largest forward activation barrier according to Table 1. This result agrees with previous works at high coverage in terms of barrier and transition state structure.[29,33,34,36] S7 is not activated at a low coverage of 1/

DOI: 10.1021/cs5012525
ACS Catal. 2015, 5, 1068−1077

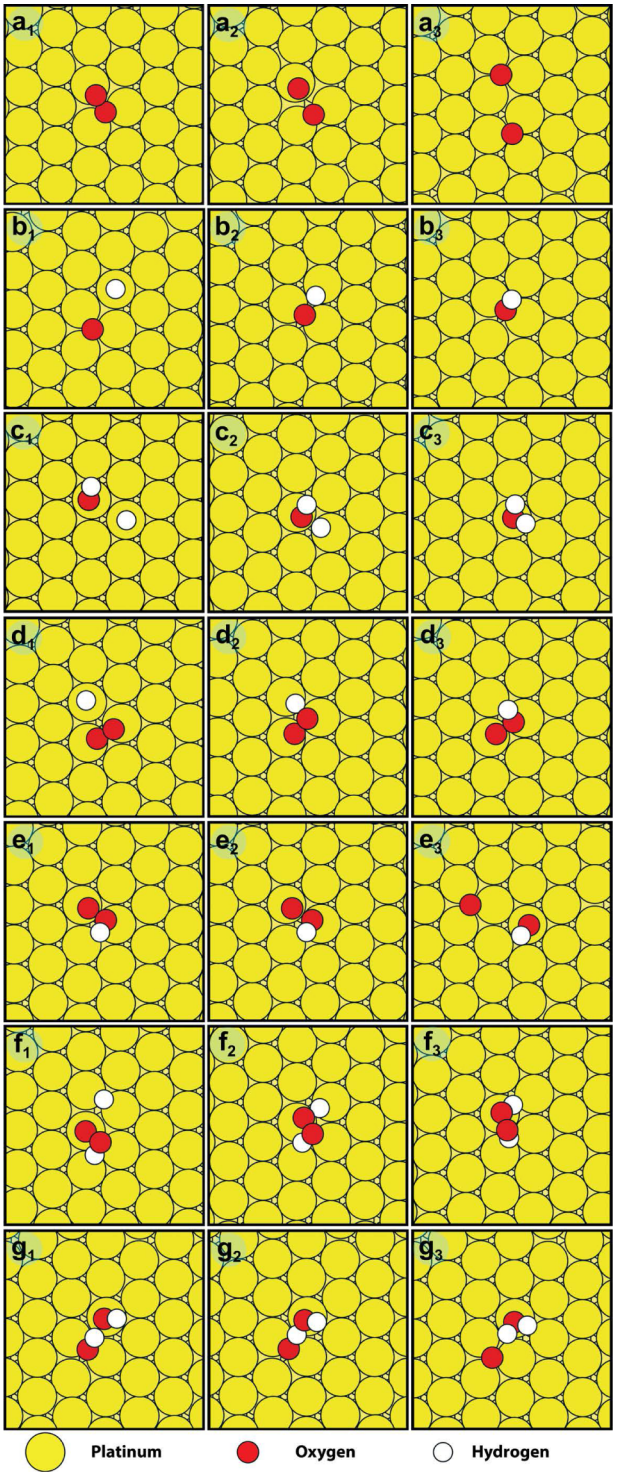

Figure 2. Top views of each elementary step ranging from *a* to *g* (*x*): *a* O_2 dissociation, *b* OH formation, *c* H_2O formation, *d* OOH formation, *e* OOH dismutation, *f* H_2O_2 formation, *g* OH disproportionation. For each elementary act, the optimal structures of initial state (x_1), transition state (x_2) and final state (x_3) are depicted. The definition of atom colors is also indicated.

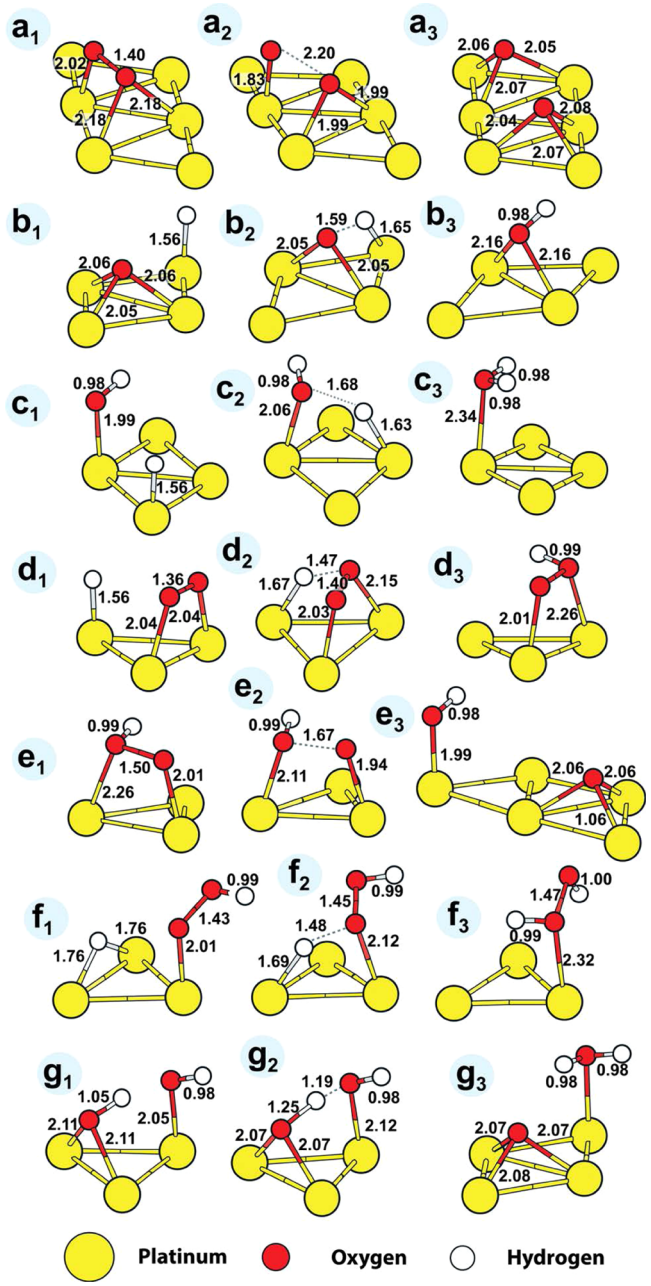

Figure 3. Lateral views of each elementary step ranging from *a* to *g* (*x*): *a* O_2 dissociation, *b* OH formation, *c* H_2O formation, *d* OOH formation, *e* OOH dismutation, *f* H_2O_2 formation, *g* OH disproportionation. For each elementary act, the optimal structures of initial state (x_1), transition state (x_2), and final state (x_3) are depicted. The definition of atom colors is also indicated.

12 ML, whereas a small barrier of 15 kJ mol^{-1} has been proposed at high coverage.[36] In our reaction mechanism, this means that hydroxyl formation would be exclusively achieved by OOH dissociation. However, in electrochemical conditions, the presence of water in the electrolyte and at the metal interface suggests a possible adsorption of this molecule. In the case of coadsorption of water with adsorbed atomic oxygen resulting from O_2 dissociation, the backward elementary step of OH disproportionation S4 (corresponding to water comproportionation) is possible. Indeed, the corresponding barrier is 24 kJ mol^{-1} according to Table 1. Hence, in this perspective, there might be a competition to form hydroxyl intermediate between OOH dismutation and water comproportionation. Our low coverage result supports the previous DFT studies at medium and high coverage[29−31,33,36]

Once hydroxyl and hydroperoxyl intermediates have been yielded on the catalyst surface, the elementary steps leading to

DOI: 10.1021/cs5012525
ACS Catal. 2015, 5, 1068−1077

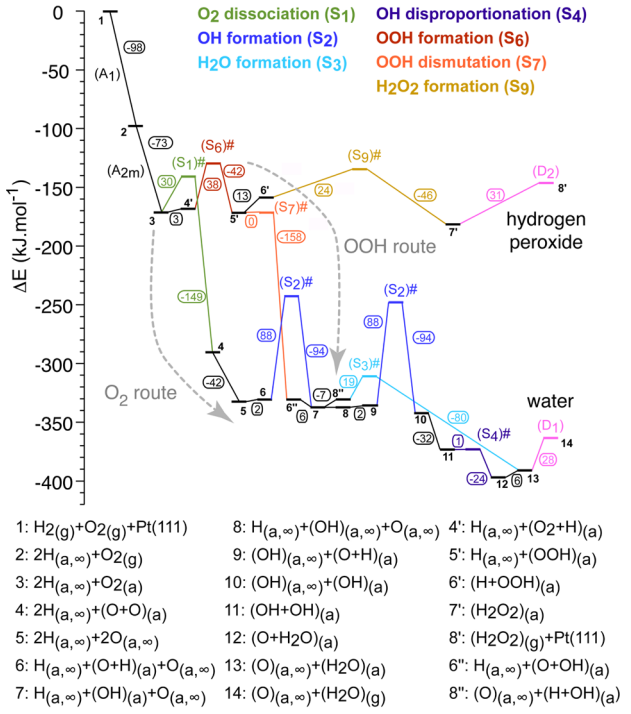

Figure 4. Total electronic energy profile (kJ mol^{-1}) for water and hydrogen peroxide formations on Pt(111) at a low coverage of 1/12 ML. The initial state (1) is a gas phase mixture of H_2 + O_2 above a clean Pt(111) surface. The two final states are gas water (14) or gas hydrogen peroxide (8′) and a clean Pt(111) surface. The subscripts (a) means adsorbed or coadsorbed state, whereas (∞) means the sum of binding energies of noninteracting adsorbates. The transition states of the elementary steps are denoted (S_i)#.

the formation of two products in competition (water and hydrogen peroxide) can be examined. At low coverage and in the absence of electrolyte, the formation of water can result from the OH + H association S3 or from the OH disproportionation S4 with respective activation barriers of 19 and 1 kJ mol^{-1}, and imaginary frequencies of 404 and 578 cm^{-1}. Our results are compatible with other works at a larger coverage with barriers of 13−21 kJ mol^{-1}[30,36] and 0−13 kJ mol^{-1}[29,33,34,36] for S3 and S4, respectively. Therefore, from the comparison with the literature, the barrier of water formation does not seem to depend on the surface coverage of the hydroxyl reactant. Subsequently, this analysis will be developed in greater detail. With respect to the formation of hydrogen peroxide, one elementary step is possible S9 according to the selected mechanism with a low coverage barrier of 24 kJ mol^{-1} and an imaginary frequency of 632 cm^{-1}, in agreement with the value of 20 kJ mol^{-1} obtained at a larger coverage.[36]

In summary, at a low coverage of 1/12 ML, the direct dissociation of molecular oxygen (30 kJ mol^{-1}) yielding atomic oxygen on the surface is slightly preferential with respect to OOH form (38 kJ mol^{-1}). However, the formation of OH from the association of atomic oxygen and hydrogen (rate-determining step of the mechanism) is not favorable (88 kJ mol^{-1}). In this condition, it means that the catalyst surface will be rapidly covered by atomic oxygen and the catalytic activity would be rather low. The second possible route leading to OH is OOH formation (38 kJ mol^{-1}) and its subsequent dismutation (no barrier). The nonactivated OOH dissociation thus closes the way leading to hydrogen peroxide so the catalyst selectivity will be clearly in favor of water. This is in agreement with RRDE (Rotating Ring Disk Electrode) experiments showing a low formation of H_2O_2 on pure platinum catalyst (max of 4% at low potential).[57]

3.2. Influence of Hydroxyl Coverage.

As rarely mentioned by a few authors,[34] the effect of surface coverage on the reactivity is expected to play a key role, although it is often not discussed in most of previous theoretical studies where a small unit cell (corresponding to a high coverage) has been considered.[30,33,36] In the following section, the influence of hydroxyl surface coverage on the activation barriers of the elementary steps of the reaction mechanism is exposed in detail. There are several ways to model the coverage effect with periodic boundary conditions. In this work, we propose to describe the surface catalyst by a large supercell and to change the surface coverage by varying the number of coadsorbed hydroxyl species at the vicinity of the active site. According to previous experimental and theoretical works,[4,21] the total surface coverage of oxygenated species on a working model electrode is 40% at 0.9 V corresponding to a mixture of adsorbed hydroxyl (most stable intermediate), water, and atomic oxygen. On the basis of DFT calculations coupled with Monte Carlo simulations, the partial coverage of those species would be 0.3, 0.2, and 0.05 ML, respectively[21] For all those reasons, only the change of coverage of the most abundant surface intermediate (hydroxyl) has been considered in the following.

As depicted in Figure 5 for some of the elementary acts, three idealistic intermediate total coverage between 1/12 and 7/12

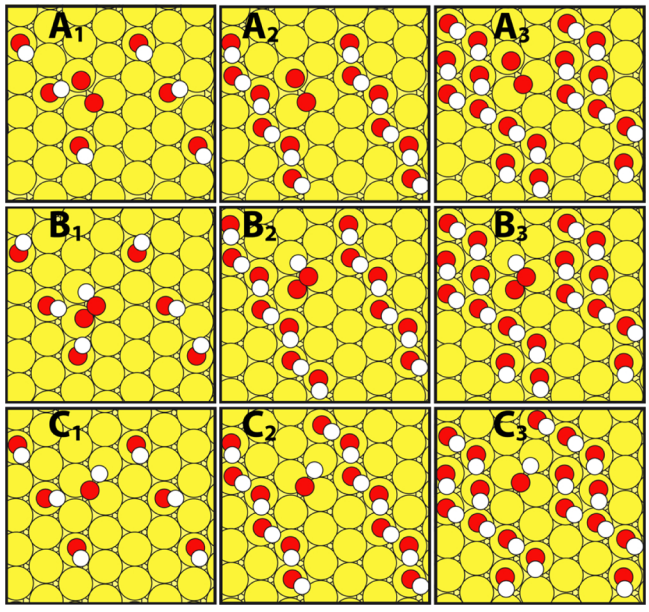

Figure 5. Top views of optimal transition state structures ranging from *A* to *C* (*X*), against hydroxyl coverage: *A* O_2 dissociation, *B* OOH formation, *C* OH formation. For each elementary step, the optimal geometries have been drawn for coadsorption with 2 OH species (X_1), 4 OH species (X_2), and 6 OH species (X_3). The definition of atom colors is the same as Figure 2.

ML have been modeled by coadsorbing 2OH (partial coverage of 1/6 ML), 4OH (1/3 ML) and 6OH species (1/2 ML) in the $(2\sqrt{3} \times 2\sqrt{3})$-R30° supercell (cf. Table 1 and the Supporting Information for the illustrations of all the elementary steps and coverage, Figures S1 to S6). Several coadsorption states have been considered by positioning those OH species on Pt(111)

DOI: 10.1021/cs5012525
ACS Catal. 2015, 5, 1068−1077

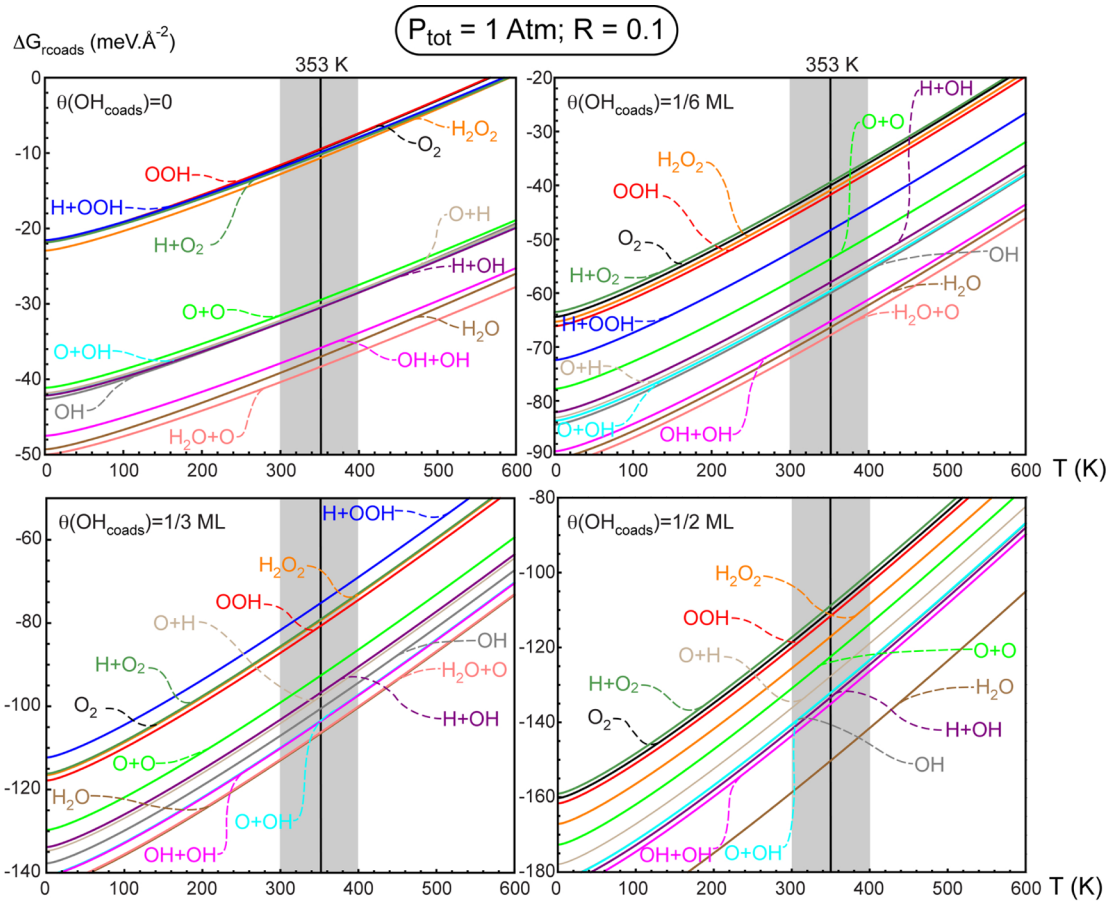

Figure 6. Reactive coadsorption Gibbs free energy diagrams ΔG_{rcoads} (meV Å^{-2}) for the most stable coadsorbed states on Pt(111) against temperature (K) and hydroxyl surface coverage (θ_{OH}) ranging from 0 to 1/2 ML. The total pressure is 1 atm and the pressure ratio between O_2 and H_2 being 0.1.

as far as possible from the reactants or the active site (spectator species) and by maximizing the stability of the complete coadsorbed layer (maximum number of hydrogen bonds between those OH species). More details about the considered arrangements and adsorption sites for hydroxyl species and optimal coadsorption structures between the reactants and those OH intermediates are available in the Supporting Information. In each case, the most stable configuration has been kept for the search of the reaction pathways. This being said, in a few cases, the interaction between the OH "spectator" species and the adsorbed reactants is stabilizing, especially for the case of 2OH in the supercell, as shown in A_1, B_1 and C_1, where several hydrogen bonds appear between them.

Regarding direct oxygen dissociation S1, an increase of the activation barrier from 30 to 51 kJ mol^{-1} (see Table 1) is obtained in agreement with the Hammond principle (progressive decrease of the exothermicity of the elementary act from −119 to −99 kJ mol^{-1}). This trend is expected due to the well-known coverage sensitivity of the final state O + O, which requires more space on the surface than the initial state O_2. So this barrier is sensitive to OH surface coverage. Nonetheless, it increases in a lesser extent than the trend previously discussed for the surface coverage of the reactant itself O_2 (from 30 to 60−74 kJ mol^{-1}). Concerning OOH formation S6, the picture is different. Neither the barrier nor the reaction energy of the elementary step changes with OH coverage. This has a consequence on the competition between direct oxygen dissociation and OOH formation. The barrier order is reversed between θ_{OH} = 1/6 and 1/3 ML. The OH formation S2 remains the rate-determining step of the mechanism with a large barrier that slightly tends to diminish when OH surface coverage increases. This is compatible with the Hammond principle because this elementary act becomes more exothermic. For the other forward barriers, the global picture is weakly modified by this change of coverage. This is also true for the majority of the backward barriers. There are two exceptions at θ_{OH} = 1/3 and 1/2 ML (S3 and S7, respectively) for which the endothermicity and the activation barrier are even larger than the values at lower coverage. As a summary, most of the elementary acts are not really sensitive to the variation of hydroxyl surface coverage, except for direct oxygen dissociation and hydroxyl formation to a lesser extent.

4. GIBBS FREE ENERGY ANALYSIS

Coming back to our initial objective, the effects of temperature and reactant pressure are now combined with those of hydroxyl surface coverage. On the basis of Gibbs free energy diagrams, exposed in Figure 6, the stability of the surface intermediates involved in the water and the hydrogen peroxide formation on Pt(111) are calculated against temperature for standard conditions of reactant pressure, for four different hydroxyl surface partial coverage: 0, 1/6, 1/3, and 1/2 ML. The zero partial coverage corresponds to the low coverage situation commented before, whereas the three other partial coverage are

DOI: 10.1021/cs5012525
ACS Catal. 2015, 5, 1068−1077

Table 2. Gibbs Free Reactive Coadsorption ΔG^{IS}_{rcoads} (for the Initial States), Reaction ΔG_{reac} and Effective Activation Energies ΔG^{eff}_{act} (kJ mol^{-1}) of Four Key Elementary Steps of Water and Hydrogen Peroxide Formations on Pt(111), against Hydroxyl Coverage (θ_{OH}, ML)[a]

elementary act	ΔG^{IS}_{rcoads} (kJ mol^{-1})				ΔG_{reac} (kJ mol^{-1})				ΔG^{eff}_{act} (kJ mol^{-1})			
θ_{OH} (ML)	0	1/6	1/3	1/2	0	1/6	1/3	1/2	0	1/6	1/3	1/2
$O_{2(ads)} + 2H_\infty \rightarrow 2O_{(ads)} + 2H_\infty$	−75	−318	−630	−874	−159	−109	−107	−98	30	31	44	51
$O_{2(ads)} + H_{(ads)} + H_\infty \rightarrow OOH_{(ads)} + H_\infty$	−81	−313	−629	−863	6	−19	−13	−22	38	40	41	44
$O_{(ads)} + H_{(ads)} + (H+O)_\infty \rightarrow OH_{(ads)} + (H+O)_\infty$	−240	−469	−777	−1013	−1	−8	−23	−36	88	90	84	80
$H_2O_{(ads)} + O_{(ads)} \rightarrow 2OH_{(ads)}$	−305	−539	−845	–	20	20	21	–	24	25	26	–

[a]These energetics have been evaluated at 353 K, a total pressure of 1 atm, and a pressure ratio between O_2 and H_2 of 0.1.

related to the 2OH, 4OH, and 6OH models exposed in the previous section.

As shown in Figure 6, 7, and in Table 2 for the key elementary steps, the successive coadsorption of ORR intermediates with OH species result in a systematic increase of the Gibbs free energy ΔG_{rcoads} from one coverage to another one. For each OH coverage, the curves of the Gibbs free energy exhibit a different slope, as explained in the Methodology section (the exponents depending explicitly on x, the number of coadsorbed OH species). However, in the considered range of temperature for fuel cell applications (around 350 K), the crossings between the curves cannot be observed (see Figure 7). If we focus the analysis on the stability of the initial states of

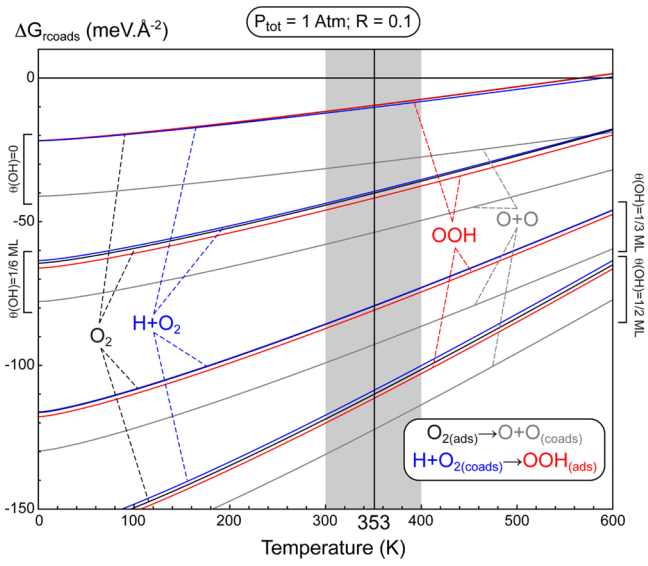

Figure 7. Reactive coadsorption Gibbs free energy diagrams ΔG_{rcoads} (meV Å^{-2}) for the two key elementary steps in competition (direct oxygen dissociation and hydroperoxyl formation on Pt(111)) against temperature (K) and hydroxyl surface coverage (θ_{OH}) ranging from 0 to 1/2 ML. The total pressure is 1 atm, and the pressure ratio between O_2 and H_2 is 0.1.

direct oxygen dissociation ($O_{2(ads)}$) and hydroperoxyl formation ($O_{2(ads)}$ + H), an inversion in the relative stability is found starting from θ_{OH} = 1/6 ML (cf. Table 2). This means that coadsorption between molecular oxygen and atomic hydrogen is destabilizing at those large coverage, in contrast with the low coverage situation. Therefore, for OOH formation, the effective activation barrier has to be calculated by summing both contributions of the crude activation energy and the diffusion barrier related to coadsorption between reactants. This explains how effective Gibbs free activation energy has been evaluated in Table 2. This will be discussed in a subsequent section. Regarding the Gibbs free reaction energy, the effects of temperature and pressure do not change the analysis exposed at zero temperature. In fact, the loss and the gain of exothermicity for direct oxygen dissociation (cf. Figure 7) and hydroxyl formation are associated with a progressive increase and decrease of Gibbs free activation energies, respectively.

The conclusion given at zero temperature is still valid at 353 K and standard pressure for competition between direct oxygen dissociation and OOH formation. As the OH coverage increases, the competition is progressively reversed in favor of OOH formation starting from θ_{OH} = 1/3 ML, as illustrated in Figure 8. If we refer to the calculated OH coverage proposed by

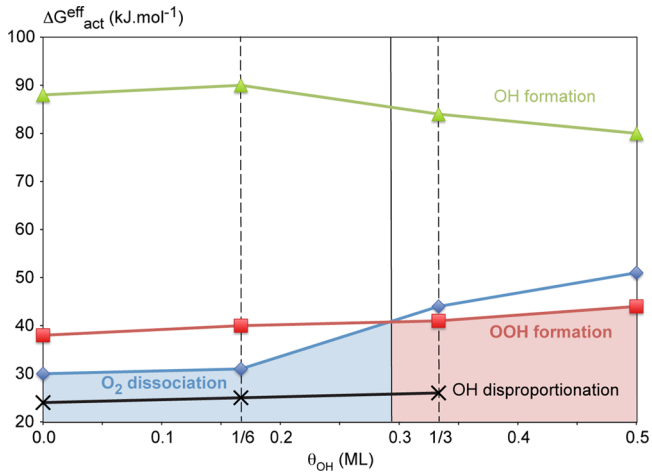

Figure 8. Effective Gibbs free activation energy diagrams ΔG^{eff}_{act} (kJ mol^{-1}) for the key elementary steps against hydroxyl surface coverage (θ_{OH}) ranging from 0 to 1/2 ML: direct oxygen dissociation, hydroperoxyl formation, OH formation and disproportionation on Pt(111). These energies have been evaluated at 353 K. For the competition between oxygen dissociation and hydroperoxyl formation, the reversing point appears around 0.3 ML. The blue area indicates that oxygen dissociation is favored at low hydroxyl coverage (from 0 to 0.3 ML), whereas the red area shows that hydroperoxyl formation is preferred at larger OH coverage (from 0.3 to 0.5 ML).

other authors on the basis of Monte Carlo simulations at 0.9 V (below 0.3 ML),[21] this would correspond in our models to coadsorption states with 4OH species (θ_{OH} = 1/3 ML). In this condition, the hydroperoxyl route is slightly preferential over the direct dissociation route. So the formation of hydroxyl and water would essentially result from OOH dismutation (low barriers). The consumption of atomic oxygen yielded by this latter dissociation would then be ensured by water comproportionation, which exhibits a low Gibbs free activation energy regardless of the OH coverage from 0 to 1/3 ML.

DOI: 10.1021/cs5012525
ACS Catal. 2015, 5, 1068−1077

In conclusion, the change of hydroxyl surface coverage has a significant impact on the reaction mechanism leading to water formation. According to our Gibbs free energy analysis, at a low OH coverage, platinum presents a low catalytic activity because the direct oxygen dissociation prevails over hydroperoxyl route in temperature and pressure operating conditions. In our gas/metal model, the catalyst surface would be rapidly poisoned by atomic oxygen (large barrier to produce OH from O). At a relevant OH coverage for fuel cell applications (1/3 ML), the picture is different. In this case, the reaction mechanism follows mainly the OOH route which yields almost exclusively OH + O through OOH dissociation (no barrier). So the formation of water would be achieved by the OH + H elementary step. In presence of aqueous electrolyte, a concomitant H_2O+O comproportionation step would transform atomic oxygen in OH. Hence, at the beginning of the reaction, water may initiate the whole catalytic mechanism by producing OH. Then, as OH surface coverage increases, the OOH route becomes preferential, hence increasing the rate leading to OH. In this perspective, hydroxyl species would be responsible for an autocatalytic process. This being said, in electrocatalytic conditions, the reaction mechanism is expected to be different, in particular with the presence of protons. This would open the way to new elementary acts that could not be examined within this model. Finally, such a competition between OOH and O_2 routes has been mentioned in the literature previously by using a DFT-based microkinetic modeling in the mean-field approximation.[58] In this work, for a constant surface coverage, the authors have shown a close competition between those two mechanisms by varying the electrode potential around 0.8 V (close to fuel cell conditions).

5. CONCLUSION

Density functional theory calculations and Gibbs free energy diagrams have been reported to explore the formation of water and hydrogen peroxide on the Pt(111) surface. A systematic and detailed analysis of the partial hydroxyl surface coverage has been proposed for the first time. The reaction mechanism has been discussed by examining three effects coming from the environment: hydroxyl coverage, temperature, and reactant pressure. According to our gas/metal model, the low OH coverage situation would favor the direct oxygen dissociation, hence limiting the catalyst activity by a high surface content of atomic oxygen. In contrast, in relevant conditions of OH coverage (around 1/3 ML), the mechanism is reversed in favor of the OOH route and subsequent dismutation leading to the formation of water. Hence, one possible role of water coming from the solvent may be to initiate the formation of hydroxyl species by comproportionation with atomic oxygen, whereas the role of hydroxyl and hydroperoxyl surface species may be to feed an autocatalytic process. This work opens perspectives to new elementary mechanisms in the presence of water and of an external electric field, on pure and alloyed metallic electrodes. Additionally, these findings are of paramount importance toward the development of multiscale models devoted to the prediction of the macroscopic fuel cell electrode performance, according to recent developments in this field.[1,59,60]

■ ASSOCIATED CONTENT

Supporting Information

The following file is available free of charge on the ACS Publications website at DOI: 10.1021/cs5012525.

Illustrations of the optimized adsorption structures of initial, transition and final states of the elementary steps involved in the reaction mechanism, as a function of surface hydroxyl coverage (PDF)

■ AUTHOR INFORMATION

Corresponding Author

*E-mail: David.Loffreda@ens-lyon.fr. Phone: +33.4.72.72.88.43. Fax: +33.4.72.72.88.60.

Notes

The authors declare no competing financial interest.

■ ACKNOWLEDGMENTS

The authors acknowledge the funding from the European Union FP7/2007-2013 program (PUMA MIND contract, Call FCH-JU-2011-1, Code SP1-JTI-FCH-2011.1.3, Grant Agreement number 303419). They warmly thank Dr Federico Calle-Vallejo for helpful discussions. They also thank IDRIS, CINES (project 609, GENCI/CT8) and PSMN for CPU time and assistance.

■ REFERENCES

(1) Franco, A. A. In *Polymer electrolyte membrane and direct methanol fuel cell technology (PEMFCs and DMFCs) - Vol. 1: Fundamentals and performance*; Hartnig, C., Roth, C., Eds.; Woodhead-Elsevier: Cambridge, U.K., 2012.
(2) Stamenkovic, V.; Schmidt, T. J.; Ross, P. N.; Markovic, N. M. *J. Phys. Chem. B* **2002**, *106*, 11970−11979.
(3) Stamenkovic, V. R.; Mun, B. S.; Mayrhofer, K. J. J.; Ross, P. N.; Markovic, N. M. *J. Am. Chem. Soc.* **2006**, *128*, 8813−8819.
(4) Stamenkovic, V. R.; Fowler, B.; Mun, B. S.; Wang, G.; Ross, P. N.; Lucas, C. A.; Markovic, N. M. *Science* **2007**, *315*, 493−497.
(5) Alayoglu, S.; Nilekar, A. U.; Mavrikakis, M.; Eichhorn, B. *Nat. Mater.* **2008**, *7*, 333−338.
(6) Wang, J. X.; Inada, H.; Wu, L.; Zhu, Y.; Choi, Y.; Liu, P.; Zhou, W.-P.; Adzic, R. R. *J. Am. Chem. Soc.* **2009**, *131*, 17298−17302.
(7) Albu, T.; Mikel, S. *Electrochim. Acta* **2002**, *52*, 3149−3159.
(8) Nørskov, J. K.; Rossmeisl, J.; Logadottir, A.; Lindqvist, L.; Kitchin, J. R.; Bligaard, T.; Jónsson, H. *J. Phys. Chem. B* **2004**, *108*, 17886−17892.
(9) Wang, Y.; Balbuena, P. B. *J. Phys. Chem. B* **2004**, *108*, 4376−4384.
(10) Filhol, J.-S.; Neurock, M. *Angew. Chem., Int. Ed.* **2006**, *45*, 402−406.
(11) Karlberg, G. S.; Rossmeisl, J.; Nørskov, J. K. *Phys. Chem. Chem. Phys.* **2007**, *9*, 5158−5161.
(12) Otani, M.; Hamada, I.; Sugino, O.; Morikawa, Y.; Okamotode, Y.; Ikeshoji, T. *Phys. Chem. Chem. Phys.* **2008**, *10*, 3609−3612.
(13) Ou, L.; Yang, F.; Liu, Y.; Chen, S. *J. Phys. Chem. C* **2009**, *113*, 20657−20665.
(14) Tripkovic, V.; Skúlasona, E.; Siahrostamia, S.; Nørskov, J. K.; Rossmeisl, J. *Electrochim. Acta* **2010**, *55*, 7975−7981.
(15) Sha, Y.; Yu, T. H.; Liu, Y.; Merinov, B. V.; Goddard, W. A. *J. Phys. Chem. Lett.* **2010**, *1*, 856−861.
(16) Skulason, E.; Tripkovic, V.; Björketun, M. E.; Gudmundsdottir, S.; Karlberg, G.; Rossmeisl, J.; Bligaard, T.; Jonsson, H.; Nørskov, J. K. *J. Phys. Chem. C* **2010**, *114*, 18182−18197.
(17) de la Hoz, J. M. M.; Leon-Quintero, D. F.; Hirunsit, P.; Balbuena, P. B. *Chem. Phys. Lett.* **2010**, *498*, 328−333.
(18) Keith, J. A.; Jerkiewicz, G.; Jacob, T. *ChemPhysChem* **2010**, *11*, 2779−2794.
(19) Callejas-Tovar, R.; Liao, W.; de la Hoz, J. M. M.; Balbuena, P. B. *J. Phys. Chem. C* **2011**, *115*, 4104−4113.
(20) Sha, Y.; Yu, T. H.; Merinov, B. V.; Shirvanian, P.; W. A. Goddard, I. *J. Phys. Chem. Lett.* **2011**, *2*, 572−576.

(21) Casalongue, H. S.; Kaya, S.; Viswanathan, V.; Miller, D. J.; Friebel, D.; Hansen, H. A.; Nørskov, J. K.; Nilsson, A.; Ogasawara, H. *Nat. Commun.* **2013**, *4*, 1−6.
(22) Bandarenka, A. S.; Hansen, H. A.; Rossmeisl, J.; Stephens, I. E. L. *Phys. Chem. Chem. Phys.* **2014**, *16*, 13625−13629.
(23) Hansen, H. A.; Viswanathan, V.; Nørskov, J. K. *J. Phys. Chem. C* **2014**, *118*, 6706−6718.
(24) Xie, T.; Hayden, C. A. *Polymer* **2007**, *48*, 5497−5506.
(25) Mittal, V. O.; Kunz, H. R.; Fenton, J. M. *J. Electrochem. Soc.* **2007**, *154*, B652−B656.
(26) Coulon, R.; Bessler, W. G.; Franco, A. A. *ECS Trans.* **2010**, *25*, 259−273.
(27) Trogadas, P.; Fuller, T. F. In *Polymer Electrolyte Fuel Cells: Science, Applications and Challenges*; Franco, A. A., Ed.; CRC Press/Taylor and Francis group: Boca Raton, FL, 2013.
(28) Eichler, A.; Hafner, J. *Phys. Rev. Lett.* **1997**, *79*, 4481−4484.
(29) Michaelides, A.; Hu, P. *J. Am. Chem. Soc.* **2000**, *122*, 9866−9867.
(30) Michaelides, A.; Hu, P. *J. Am. Chem. Soc.* **2001**, *123*, 4235−4242.
(31) Michaelides, A.; Hu, P. *J. Chem. Phys.* **2001**, *114*, 513−519.
(32) Gambardella, P.; Sljivancanin, Z.; Hammer, B.; Blanc, M.; Kuhnke, K.; Kern, K. *Phys. Rev. Lett.* **2001**, *87*, 056103−1,4.
(33) Kandoi, S.; Gokhale, A.; Grabow, L.; Dumesic, J.; Mavrikakis, M. *Catal. Lett.* **2004**, *93*, 93−100.
(34) Qi, L.; Yu, J.; Li, J. *J. Chem. Phys.* **2006**, *125*, 054701.
(35) Jacob, T.; Goddard, W. A. *ChemPhysChem* **2006**, *7*, 992−1005.
(36) Ford, D. C.; Nilekar, A. U.; Xub, Y.; Mavrikakis, M. *Surf. Sci.* **2010**, *604*, 1565−1575.
(37) Ohma, A.; Ichiya, T.; Fushinobu, K.; Okazaki, K. *Surf. Sci.* **2010**, *604*, 965−973.
(38) Nilekar, A. U.; Mavrikakis, M. *Surf. Sci.* **2008**, *602*, L89−L94.
(39) Eichler, A.; Mittendorfer, F.; Hafner, J. *Phys. Rev. B* **2000**, *62*, 4744−4755.
(40) Gu, Z.; Balbuena, P. B. *J. Phys. Chem. C* **2007**, *111*, 9877−9883.
(41) Pillay, D.; Johannes, M. *Surf. Sci.* **2008**, *602*, 2752−2757.
(42) Kresse, G.; Hafner, J. *Phys. Rev. B* **1993**, *47*, 558−561.
(43) Kresse, G.; Furthmüller, J. *Comput. Mater. Sci.* **1996**, *6*, 15−50.
(44) Kresse, G.; Furthmüller, J. *Phys. Rev. B* **1996**, *54*, 11169−11186.
(45) Perdew, J. P.; Burke, K.; Ernzerhof, M. *Phys. Rev. Lett.* **1996**, *77*, 3865−3868.
(46) Kresse, G.; Joubert, D. *Phys. Rev. B* **1999**, *59*, 1758−1775.
(47) Monkhorst, H. J.; Pack, J. D. *Phys. Rev. B* **1976**, *13*, 5188−5192.
(48) Henkelman, G.; Uberuaga, B. P.; Jonsson, H. *J. Chem. Phys.* **2000**, *113*, 9901−9904.
(49) Sheppard, D.; Terrell, R.; Henkelman, G. *J. Chem. Phys.* **2008**, *128*, 134106.
(50) P. Fleurat-Lessard Dayal, P.; . Code freely available online: http://perso.ens-lyon.fr/paul.fleurat-lessard/ReactionPath.html.
(51) Loffreda, D.; Jugnet, Y.; Delbecq, F.; Bertolini, J. C.; Sautet, P. *J. Phys. Chem. B* **2004**, *108*, 9085−9093.
(52) Loffreda, D. *Surf. Sci.* **2006**, *600*, 2103−2112.
(53) Xu, Y.; Ruban, A. V.; Mavrikakis, M. *J. Am. Chem. Soc.* **2004**, *126*, 4717−4725.
(54) Hyman, M. P.; Medlin, J. W. *J. Phys. Chem. B* **2006**, *110*, 15338−15344.
(55) Stipe, B. C.; Rezaei, M. A.; Ho, W.; Gao, S.; Persson, M.; Lundqvist, B. I. *Phys. Rev. Lett.* **1997**, *78*, 4410−4413.
(56) Nolan, P. D.; Lutz, B. R.; Tanaka, P. L.; Davis, J. E.; Mullins, C. B. *J. Chem. Phys.* **1999**, *111*, 3696−3704.
(57) Sethuramana, V.; Weidnera, J.; Haugb, A.; Pembertonb, M.; Protsailo, L. *Electrochim. Acta* **2009**, *54*, 5571−5582.
(58) Keith, J. A.; Jacob, T. *Angew. Chem., Int. Ed.* **2010**, *49*, 9521−9525.
(59) de Morais, R. F.; Sautet, P.; Loffreda, D.; Franco, A. A. *Electrochim. Acta* **2011**, *56*, 10842−10856.
(60) Eberle, D.; Horstmann, B. *Electrochim. Acta* **2014**, *137*, 714−720.

DOI: 10.1021/cs5012525
ACS Catal. 2015, 5, 1068−1077